Available online at www.sciencedirect.com
SCIENCE DIRECT
Journal of Catalysis 238 (2006) 232–241
JOURNAL OF CATALYSIS
www.elsevier.com/locate/jcat

n-Butane oxidation over VPO catalysts supported on SBA-15

Xiu-Kai Li [a,b], Wei-Jie Ji [b,*], Jing Zhao [b], Zhi-Bing Zhang [b], Chak-Tong Au [a,*]

[a] *Department of Chemistry, Center for Surface Analysis and Research, Hong Kong Baptist University, Kowloon Tong, Hong Kong, China*
[b] *Key Laboratory of Mesoscopic Chemistry, Ministry of Education, Department of Chemistry, Nanjing University, Nanjing 210093, PR China*

Received 28 July 2005; revised 24 November 2005; accepted 11 December 2005

Abstract

VPO catalysts supported on SBA-15 were prepared by adopting a deposition–precipitation method based on organic phases. The unique properties of SBA-15, such as high surface area, large pore volume, and large pore size, enable good dispersion of VPO species in crystalline form. A mixture of iso-butyl/benzyl alcohols is more suitable than a single iso-butanol phase for the loading of VPO, and crystallized $(VO)_2P_2O_7$ was the species predominantly deposited on SBA-15 with high dispersion. At 673 K, the obtained MA yields were 51, 44, and 30% over the 60, 45, and 30 wt% VPO/SBA-15 catalysts, respectively. Techniques such as N_2 adsorption–desorption measurement, XRD, TEM, XPS, Raman spectroscopy, and H_2-TPR were adopted to explore the nature of the catalysts and to understand the characteristics of the supported VPO components. Based on the results of characterization and evaluation, a correlation between catalyst structure and performance was established.

Keywords: SBA-15; Supported VPO; Partial oxidation; *n*-Butane; Maleic anhydride

1. Introduction

Vanadium phosphorus oxide (VPO) catalysts composed mainly of vanadyl pyrophosphate ($(VO)_2P_2O_7$) are effective for the oxidation of *n*-butane to maleic anhydride (MA) [1–3]. This is in fact the only industrialized process for the oxidation of light alkanes. Despite the extensive work devoted to understanding the peculiar properties of VPOs [4–11], certain aspects (e.g., the form of active phase [12–15] and the nature of active sites [16–18]) are still subject to debate.

Potentially, supported VPO catalysts have advantages over the unsupported ones, including better heat transfer character, larger surface area to volume ratio of active component, better mechanical strength, and controllable catalyst textures. Such materials as SiO_2, TiO_2, Al_2O_3, and SiC have been used in attempts to support VPO [19–28]. It turns out that using a support can result in support–oxide interaction that may hinder the formation of $(VO)_2P_2O_7$ phase or bring about changes in phase composition [20,26,27]. It has been reported that V^{5+}-containing phase, such as α_1-$VOPO_4$ or γ-$VOPO_4$, exists in supported VPO catalysts, especially in those prepared in aqueous media, and that the presence of such phases may lower *n*-butane conversion and/or MA selectivity [19,23,25].

SBA-15 and MCM-41 are silica-based mesoporous materials with well-ordered hexagonal porosity and high thermal stability and surface area [29–31]. Nie and coworkers [32,33] supported VPO on Al-containing MCM-41 and observed significant improvement in MA selectivity. Compared with MCM-41, SBA-15 has thicker pore walls and larger pores that are responsible for higher thermal stability, higher capacity for loading supported components, and lower limitation of internal mass transfer. We postulate that better VPO dispersion and improved catalytic performance can be achieved by adopting SBA-15 as a support.

The method used to prepare VPO catalysts can be classified according to the type of medium adopted for catalyst generation: aqueous or organic. It is generally recognized that VPO catalysts prepared in an organic medium perform better than those prepared in an aqueous medium [34]. In the case of organic medium, iso-butanol usually has been adopted as a solvent [8,15,35–39], and in some cases a stronger reducing agent (commonly benzyl alcohol) also has been added [40–42]. As

* Corresponding authors. Fax: +852 3411 7348.
E-mail addresses: jiwj@nju.edu.cn (W.-J. Ji), pctau@hkbu.edu.hk (C.-T. Au).

0021-9517/$ – see front matter
doi:10.1016/j.jcat.2005.12.012

reported in the literature, most research has focused on the preparation chemistry of unsupported VPOs, and the chemistry involved in the synthesis of supported VPOs merits investigation.

The present study is the first to adopt SBA-15 as a support material for VPO dispersion and to investigate the influence of preparation medium and VPO loading on the nature of supported VPOs. The physicochemical properties of SBA-15-supported VPO catalysts were systematically examined by XRD, TEM, Raman, XPS, N_2 adsorption–desorption, and H_2-TPR.

2. Experimental

2.1. Catalyst preparation

The SBA-15 material was synthesized according to the well-established LCT method [31]. Both single iso-butanol and mixed iso-butyl/benzyl alcohols were adopted as preparation media for VPO loading. In the case of single iso-butanol, V_2O_5, H_3PO_4 (85%), PEG 6000, and SBA-15 were added to iso-butanol (21.2 ml of alcohol/g V_2O_5; atomic P/V ratio = 1.2/1). The mixture was refluxed at 378 K for 16 h, and a light blue suspension was obtained. The solid was filtered out and washed with iso-butanol and acetone, and the product obtained was dried in air at 393 K for 24 h.

VPO loading in the mixed iso-butyl/benzyl alcohols was performed as described previously [43]. V_2O_5 was first refluxed in a mixture of iso-butyl/benzyl alcohols (volume ratio of 1:1) at 413 K for 5 h, after which PEG 6000 and SBA-15 materials were introduced in suitable amounts. One hour later, phosphoric acid (85%) was added dropwise to reach a P/V atomic ratio of 1.2/1.0. After another 6 h of refluxing, the suspension was filtered and the solid was washed with iso-butanol and acetone, respectively, then further dried in air at 393 K for 24 h. The material thus obtained was the precursor of supported vanadyl pyrophosphate. Before characterization and performance evaluation, all of the samples were in situ activated according to the following procedure. The dried precursor was heated from room temperature (RT) to 673 K at a rate of 2 K/min in the reaction mixture (1.5% *n*-butane/air) and kept at this temperature for at least 12 h. The samples prepared using a "single alcohol" of iso-butanol are denoted as VPO/SBA-15(s) and VPO(s), whereas those prepared using mixed alcohols are denoted as VPO/SBA-15(m) and VPO(m).

2.2. Catalyst evaluation

Catalytic performance for the partial oxidation of *n*-butane to MA was evaluated in a quartz fixed-bed microreactor (Φ = 8 mm) with a continuous reactant downflow. The samples were pressed into pellets and then crushed and sieved to 25–40 mesh. Typically, 0.5 g of sample was charged into the reactor. The feed composition was 1.5% n-C_4H_{10}, 17.5% O_2 (in volume), and balance N_2. The gas hourly space velocity (GHSV) was ca. 1200 h^{-1}. On-line gas chromatography was used to analyze the outlet effluent; the carbon balance was usually >95%.

2.3. Characterization

Powder X-ray diffraction was conducted using a Rigaku automatic diffractometer (Rigaku D-MAX) with monochromatized Cu-K_α radiation ($\lambda = 0.15406$ nm) at a setting of 30 kV. The BET surface areas and pore structures were measured by means of a NOVA-1200 material physical structure determinator. The samples were degassed at 573 K for 3 h, after which N_2 adsorption was conducted at 77 K. Raman spectra were collected using a LABRAM-HR Raman spectrometer at RT with excitation source of 513 nm and power of 1.0 mW. XPS measurement was performed using a VG CLAM 4 MCD Analyzer X-ray photoelectron spectrometer with 1253.6 eV (Mg-K_α) radiation at settings of 10 kV and 15 mA. The binding energies (BEs) were calibrated against the C1s signal (284.6 eV) of contaminant carbon. The surface concentrations of elements were estimated on the basis of the corresponding peak areas being normalized using the Wagner Factor database. The TEM images were obtained with a TEM-200CX transmission electron microscope. Temperature-programmed reduction (TPR) was carried out in the temperature range 303–1273 K. The sample (50 mg) was reduced in 5% H_2/Ar (40 ml/min) at a rate of 10 K/min.

3. Results

3.1. Characterization

3.1.1. Physical property

The N_2 adsorption–desorption profiles of VPO/SBA-15 catalysts are illustrated in Figs. 1 and 2, with the related data given in Table 1. As shown in Fig. 1, all of the supported catalysts exhibited type IV isotherms with a sudden increase in volume of gas uptake within the relative pressure (P/P_0) range of approximately 0.6–0.8, signifying typical mesoporous structures of uniform pore size. Fig. 2 depicts the pore size distributions of the catalysts. The pore size of SBA-15 maximized at ca. 8.3 nm, notably higher than the value (5.0 nm) calculated based on the BJH method (Table 1). The micropores on the walls of meso-

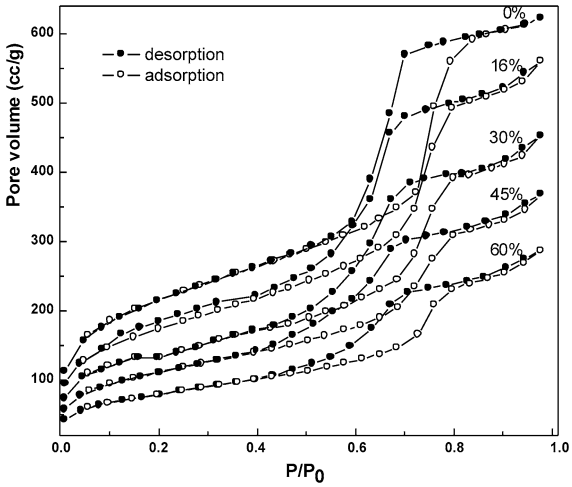

Fig. 1. N_2 adsorption–desorption isotherms of VPO/SBA-15(m) catalysts.

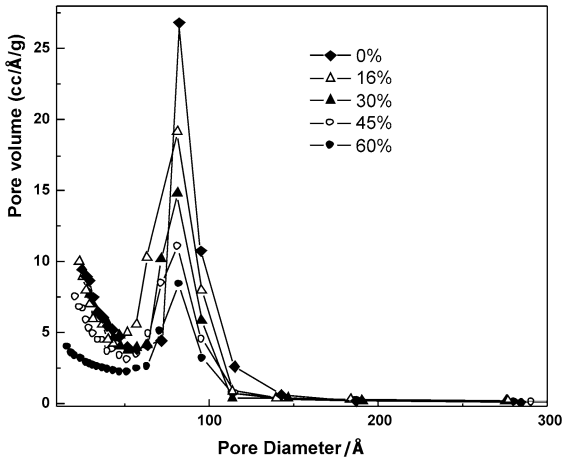

Fig. 2. Pore size distribution of VPO/SBA-15(m) catalysts.

Table 1
The characteristics of SBA-15 and VPO/SBA-15 catalysts

Sample	S_{BET} (m^2/g)	Pore volume (cm^3/g)	Pore diameter (Å)
Bulk VPO(m)	30	–	–
Bulk VPO(s)	8	–	–
60% loading(m)	283	0.44	62.4
45% loading(m)	396	0.56	57.4
45% loading(s)	304	0.45	59.7
30% loading(m)	464	0.70	60.3
16% loading(m)	620	0.87	55.9
SBA-15	762	0.96	50.4

pores of SBA-15 might account for the lower average SBA-15 pore diameter [44,45]. As shown in Table 1, the average pore diameter of samples increased with increasing VPO loading. This finding is understandable, because during VPO loading, the micropores were readily plugged by the VPO components and were not included in the measurement. This is also confirmed by the profile of pore size distribution shown in Fig. 2, showing that the volume of micropores decreased significantly with increasing VPO loading. In contrast, the preparation medium had a notable impact on the sample characteristics. The surface area (8 m^2/g) of VPO(s) (prepared in single alcohol) was much lower than that (30 m^2/g) of VPO(m) (prepared in mixed alcohols). Structural differences between the supported 45%VPO/SBA-15(s) and 45%VPO/SBA-15(m) catalysts are also obvious; the former was lower in both surface area and in pore volume.

3.1.2. XRD

Fig. 3A shows the small-angle XRD patterns of SBA-15 and VPO/SBA-15 samples of different VPO loadings. The SBA-15 support showed three well-resolved Bragg peaks at $2\theta = 0.77°$, 1.57°, and 1.86°, corresponding to the diffraction of (100), (110), and (200) planes. These peaks are characteristics of the hexagonally ordered structure of SBA-15 [31]. With successive loading of VPO onto SBA-15, the d_{100} peak disappeared gradually, whereas the d_{110} and d_{200} peaks attenuated in intensity. Such observation can be ascribed to the partial blocking

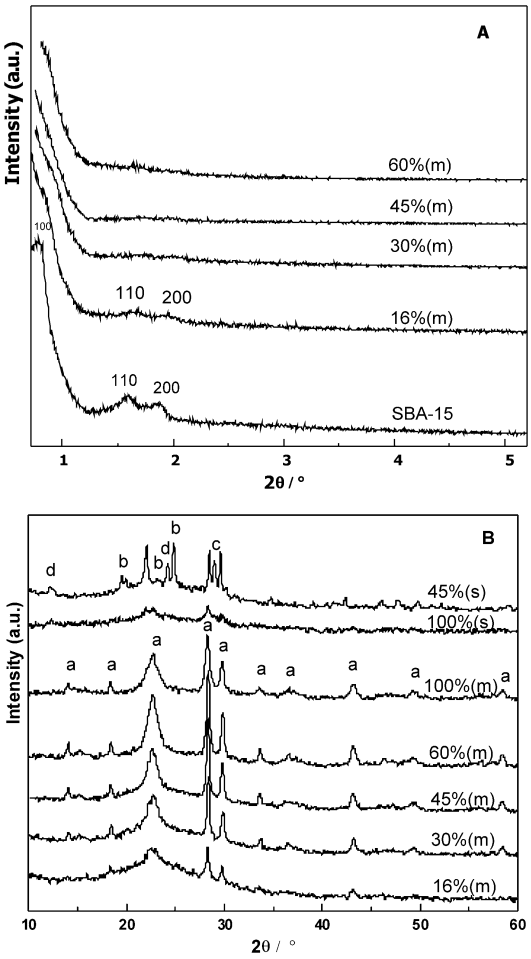

Fig. 3. Small-angle (A) and wide-angle (B) XRD patterns of VPO/SBA-15 catalysts at various VPO loadings; the wide-angle XRD patterns of VPO(m) and VPO(s) are also shown for comparison. a: $(VO)_2P_2O_7$; b: γ-$VOPO_4$; c: α_1-$VOPO_4$; d: $VOPO_4{\cdot}2H_2O$.

of SBA-15 mesopores by VPO species and the notable loss in long-range order of hexagonally arranged porosity [46,47]. The wide-angle XRD patterns of VPO and VPO/SBA-15 (Fig. 3B) showed that the supported VPO species existed in the form of crystalline $(VO)_2P_2O_7$ even at VPO loading as low as 16 wt%. Poor intensity of the diffraction peaks at low VPO loadings could be a result of structural disorder and/or silica interference [28].

The type of medium used in the preparation could have a significant impact on the nature of the supported VPO component. Compared with VPO(m), the VPO(s) sample had a vanadyl pyrophosphate phase of lower crystallinity. The 45%VPO/SBA-15(s) catalyst showed not only poor crystallinity, but also the existence of V^{5+}-containing phases ($VOPO_4{\cdot}2H_2O$, α_1-$VOPO_4$, and γ-$VOPO_4$) in large proportion. These V^{5+}-containing phases were also observed in the VPO catalysts supported on conventional SiO_2 prepared in aqueous media [19,23,25]. The difference in phase composition of supported VPO catalysts could originate from the formation of VPO precursor. Fig. 4 shows the XRD patterns of selected precursors prepared in single alcohol and mixed alcohols. Both VPO(s) and 45%VPO/SBA-15(s) showed high crystallinity, as reflected

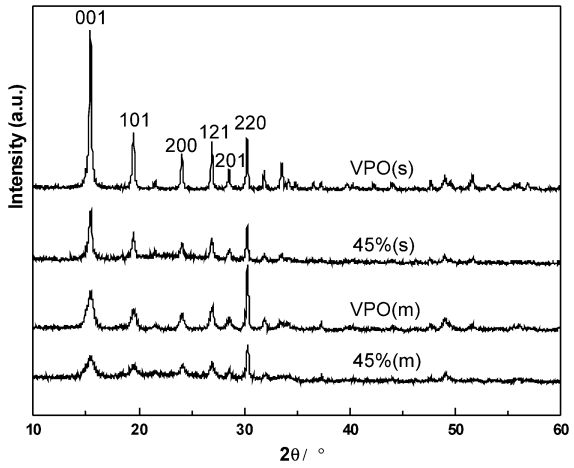

Fig. 4. XRD patterns of selected precursors generated in different organic media.

by the narrow and intense (001) diffraction peak ($2\theta = 15.4°$). However, the precursors prepared in mixed alcohols exhibited significant structure disorder, owing to the intercalation of aromatic molecules into the precursor materials [1,2,5,7,41].

3.1.3. TEM

The (HR)TEM images shown in Fig. 5 are the images of the VPO/SBA-15 samples viewed from two different directions. Figs. 5A and 5C are images viewed from a direction parallel to the channels, whereas Fig. 5B is image viewed from a perpendicular direction. From Figs. 5A and 5C, one can see whether any VPO components are located inside the channels as well as at the pore mouths, whereas from Fig. 5B, one can determine whether the VPO components are located on the external surface or inside the mesopores of SBA-15. As revealed by the HRTEM image (Fig. 5B) of a sample of low (16%) VPO loading, the VPO components existed as rod-like entities (5–8 nm diameter, 30–60 nm long) rather than as massive VPO particles of irregular shapes. The image shows both empty and filled channels. Looking at the HRTEM images of the pore mouths of the 30%VPO/SBA-15 sample (Fig. 5C), one can also see that some channels were filled with VPO components, whereas some were not. Based on the results of TEM and HRTEM investigations, it seems reasonable to conclude that there were VPO components inside the mesopores of SBA-15. However, it should be mentioned that there could be VPO particles on the external surface of the support as well even at low VPO loading (e.g., 16%). Increased VPO loading should increase the likelihood of having VPO entities located outside the channels. Based on Fig. 3B, the crystallite size of VPO particles of the activated samples was estimated as >20 nm (using Scherrer's formula). Bear in mind that the estimation is an overall effect of the VPO components in different sizes, that is, those on the external surface (relatively larger in size) as well as those inside the mesopores (i.e., the nanorod VPO entities). A large overall crystallite size does not exclude the possibility of having the XRD signals being partly contributed by the nanorod VPO entities located inside the SBA-15 channels.

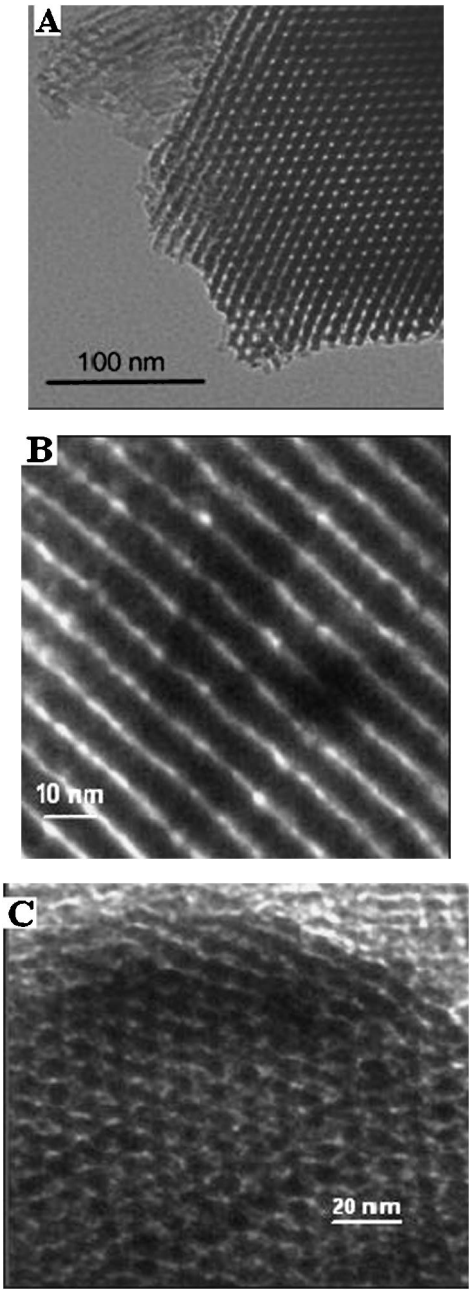

Fig. 5. Representative TEM images of the activated VPO/SBA-15(m) catalysts. (A) and (B) 16%VPO/SBA-15(m); (C) 30%VPO/SBA-15(m).

This assumption is in accordance with the results of small-angle XRD, pore distribution, and TPR studies (see later). The results of our previous study indicated that with the addition of PEG additive in the preparation medium, the unsupported VPO showed considerably higher surface area (in the range of 40–70 m^2/g) and features of fine particles [9]. In the case of VPO/SBA-15 at high VPO loadings, the particle size of the VPO entities present on the external surface of support should be comparable to or even smaller than that of unsupported PEG-derived VPO. With extensive plugging of the pores at high VPO loadings, the XRD peaks of (100), (110), and (200) diffraction characteristic of the ordered hexagonal mesostructure diminished notably, as shown in Fig. 3A.

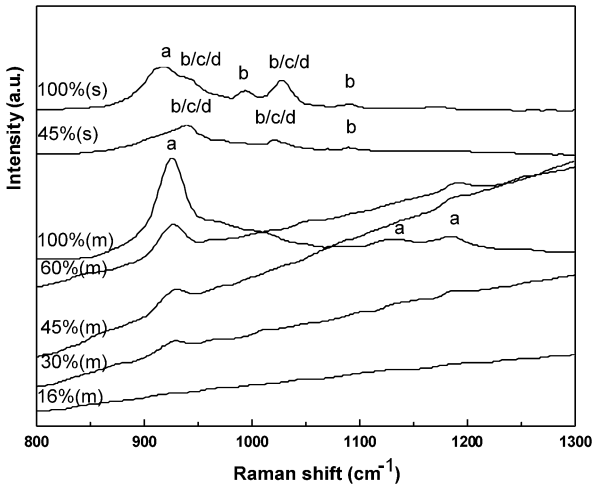

Fig. 6. Raman spectra of VPO and VPO/SBA-15 catalysts. a: $(VO)_2P_2O_7$; b: γ-$VOPO_4$; c: α_1-$VOPO_4$; d: $VOPO_4{\cdot}2H_2O$.

3.1.4. Raman spectroscopy

Fig. 6 shows the Raman spectra of VPO and VPO/SBA-15 samples. For the samples prepared in mixed alcohols, the spectrum of unsupported VPO shows three well-resolved Raman bands at 925, 1132, and 1185 cm^{-1}. The major band at ca. 925 cm^{-1} can be attributed to ν(as) P–O–P in the $P_2O_7^{2-}$ unit of $(VO)_2P_2O_7$, and the rather weak bands at 1132 and 1185 cm^{-1} are characteristic of the $(VO)_2P_2O_7$ species [8,9,28,43]. No signal related to V^{5+}-containing species could be identified. Due to the interference of silica [28,43], Raman signals decreased in intensity with decreasing VPO loading. The Raman spectra of VPO(s) and 45%VPO/SBA-15(s) differ remarkably from those of VPO(m) and VPO/SBA-15(m). The broad band within the 920–960 cm^{-1} region indicates the coexistence of pyrophosphate and orthophosphate (γ-$VOPO_4$, α_1-$VOPO_4$ and $VOPO_4{\cdot}2H_2O$) phases; the bands at 994 and 1028 cm^{-1} further confirm the presence of V^{5+}-containing species in large proportion [8,9,28,43]. The results of the Raman study are in good agreement with those of the XRD examination (Fig. 3B).

3.1.5. XPS

XPS analysis can provide information related to oxidation state and concentration of surface elements. As shown in Table 2, The $V2p_{3/2}$ BEs of VPO(m), VPO(s), and VPO/SBA-15(m) are around 517.2 eV, close to that (517.6 eV) reported for well-crystallized $(VO)_2P_2O_7$ [9,48] but lower than that reported for vanadium pentoxide and V(IV) phosphate [48,49]. Hence the vanadium oxidation states of these catalysts are approximately 4+, and the VPO components are in the form of $(VO)_2P_2O_7$. The $V2p_{3/2}$ binding energy of 45%VPO/SBA-15(s) is 518.2 eV, ca. 1 eV higher than those of other samples; thus the oxidation state is considered close to 5+. The O1s binding energies of the supported VPO catalysts are appreciably higher than those of unsupported ones, due mainly to the contribution of the support itself (see the BE of pure SBA-15 in Table 2). The P2p binding energies of surface phosphate are very similar (ca. 133.7 eV) for all of the samples. A surface enrichment of P element was observed over all of the samples; this

Table 2
XPS results of SBA-15 and VPO/SBA-15 catalysts

Sample	$V2p_{3/2}$ (eV)	P2p (eV)	O1s (eV)	Surface composition (at%)					
				V	P	O	Si	P/V	Si/V
Bulk VPO(m)	517.3	133.7	531.4	10.2	15.9	73.9	–	1.6	–
Bulk VPO(s)	517.1	133.6	531.6	13.7	22.4	63.9	–	1.6	–
60% loading(m)	517.1	133.9	532.7	4.1	6.3	72.2	17.5	1.5	4.3
45% loading(m)	517.2	133.9	532.6	3.0	4.2	73.7	19.1	1.4	6.4
45% loading(s)	518.2	133.8	532.9	2.1	2.9	76.1	18.8	1.4	8.8
30% loading(m)	517.4	134.0	532.8	2.1	3.2	73.6	21.1	1.5	10.0
16% loading(m)	517.1	133.7	532.8	1.4	2.0	62.6	34.0	1.4	24.3
SBA-15	–	–	532.9	–	–	–	–	–	–

is a common phenomenon for both supported and unsupported VPO catalysts [9,20,21,38,48]. A slight "excess" of surface P is believed to stabilize the active phase and favor the formation of MA [48,50]. An in situ XPS study of a working VPO catalyst revealed that the surface P/V and O/V ratios varied with feed composition and reaction temperature, indicating that different active sites were involved in the catalytic oxidation of *n*-butane [17].

The ratio of surface vanadium to silicon can be considered a function of the degree of VPO coverage [20,33]. From Table 2, one can see that the surface V:Si ratio increased with increasing VPO loading over the serial VPO/SBA-15(m) catalysts, as a result of attenuation of the Si signals by the loaded VPO. The surface Si:V ratio decreased drastically from 24.3 to 10.0 with increased VPO loading from 16 to 30%, indicating that the amount of VPO component existing outside of the pores increased with increasing VPO loading, as observed in the TEM studies (Fig. 5). The Si:V ratio of 45%VPO/SBA-15(m) is lower than that of 45%VPO/SBA-15(s), implying that the former showed better VPO dispersion on the external surface of SBA-15.

3.1.6. H_2-TPR

Fig. 7 reports the reduction behaviors of the bulk and supported VPO catalysts. For the samples prepared in mixed alcohols, the TPR profiles showed one main peak at temperatures above 730 °C, attributable to the removal of lattice oxygen related to V^{4+} species in the $(VO)_2P_2O_7$ phase. The dispersion state showed a notable effect on the reduction behavior of the supported VPO component. At 16 and 30% VPO loadings, the reduction profiles were similar and the reduction peak maximized at ca. 731 °C; at 45 and 60% VPO loadings, the major TPR peaks increased by ca. 20 °C. As mentioned earlier, for the samples with VPO loadings <30%, some of the VPO components were located inside the pores of SBA-15 and were dispersed in small dimensions, and hence they are more readily reduced. Above 30% VPO loading, VPO components were located predominantly on the external surface of SBA-15, and the VPO particles were larger and more "bulk-like"; hence the reduction behavior resembled that of unsupported VPO.

Unlike the TPR profiles of VPO(m) and VPO/SBA-15(m), those of VPO(s) and 45%VPO/SBA-15(s) showed reduction peaks below 600 °C, attributable to the removal of lattice oxygen related to V^{5+} species [9,43]. Compared with the major

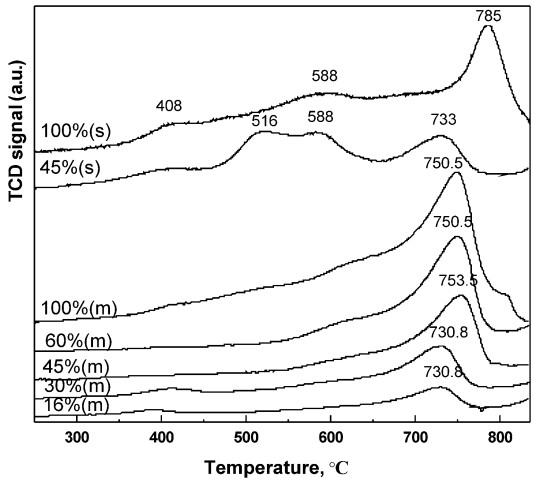

Fig. 7. Temperature-programmed reduction (TPR) profiles of VPO and VPO/SBA-15 catalysts.

reduction peak of VPO(m) at 751 °C, that of VPO(s) was ca. 34 °C higher, indicating that the lattice oxygen was relatively less reactive. The reduction profile of 45%VPO/SBA-15(s) differed appreciably from those of the other samples, because the majority of supported VPO existed as vanadium orthophosphates, as revealed in XRD (Fig. 3) and Raman (Fig. 6) investigations.

3.2. Catalytic activity

3.2.1. The effect of preparation media

Fig. 8 shows the catalytic performance observed over VPO(m) and VPO(s) as well as over 45%VPO/SBA-15(m) and 45%VPO/SBA-15(s). In the case of unsupported catalysts, VPO(m) was superior to VPO(s) in terms of MA selectivity and particularly *n*-butane conversion. It is reasonable to ascribe the lower activity of the latter to lower surface area (Table 1) and less reactive lattice oxygen (Fig. 7). As for the supported catalysts, 45%VPO/SBA-15(m) performed better than 45%VPO/SBA-15(s) in both MA selectivity and *n*-butane conversion. The results can be ascribed to the discrepancy in structural feature between the two catalysts.

3.2.2. The effect of VPO loading

Fig. 9A shows that at identical reaction temperatures, *n*-butane conversion increased significantly with increasing VPO loading. As shown in Fig. 9B, MA selectivity decreased at elevated temperatures owing to the consecutive oxidation of MA to carbon oxides. At equal reaction temperatures, MA selectivity increased with increasing VPO loading, in accordance with the findings for the silica-supported VPO catalysts [20,43]. It is possible that at higher VPO dispersion (i.e., lower VPO loading), there are more reactive oxygen adspecies that are responsible for the formation of CO_x [51], and thus MA selectivity is lower at low VPO loading.

Fig. 9C plots MA selectivity as a function of *n*-butane conversion. One can see that MA selectivity decreased with increasing *n*-butane conversion, due to the need for higher temperatures for higher conversion. In general, the serial VPO/SBA-15 catalysts showed fairly high *n*-butane conversion while maintaining better MA selectivity and consequently giving high MA yields. The typical MA yields at 673 K were 51, 44, and 30% over the 60, 45, and 30% VPO-loaded catalysts, respectively. The catalyst performance of the VPO/SBA-15 samples was superior to that of VPO catalysts supported on Al-MCM-41 [32,33], TiO_2 [21], and large-pore silica [32] and comparable with those of VPO species on fumed SiO_2 [28] and on SiO_2 generated by means of electrochemical deposition [20].

Fig. 10 plots the specific activities normalized to per unit mass of loaded VPO. The catalytic activity essentially increased with decreasing VPO loading (i.e., increasing VPO dispersion), because more active sites were available at higher dispersion on the basis of per unit mass of VPO component. As shown in Fig. 11, at temperatures above 633 K, the MA formation rate on the basis of per unit mass of VPO also increased with increasing VPO dispersion.

4. Discussion

4.1. The effect of preparation medium

The results of characterization clearly reveal that the preparation medium exhibited a significant influence on the nature of VPO (both supported and unsupported) and, consequently, on

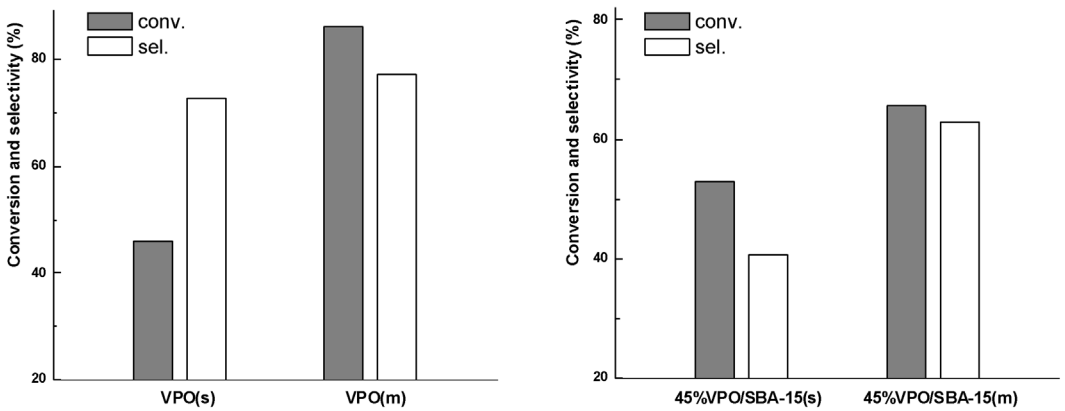

Fig. 8. The catalytic performance at 653 K over VPO(m) and VPO(s) as well as 45%VPO/SBA-15(m) and 45%VPO/SBA-15(s) catalysts.

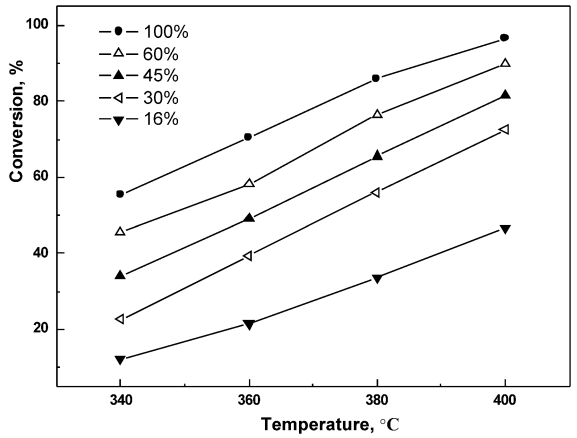

(A)

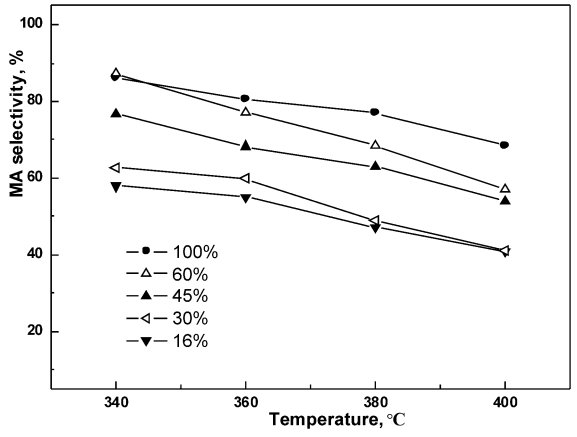

(B)

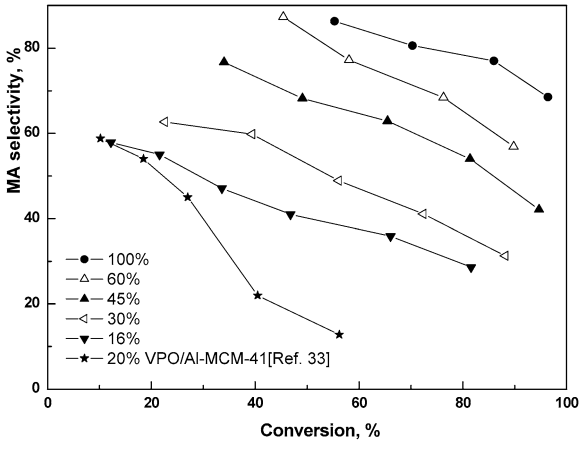

(C)

Fig. 9. (A) *n*-Butane conversion and (B) MA selectivity as a function of reaction temperature, and (C) MA selectivity as a function of butane conversion over VPO(m) and VPO/SBA-15(m) catalysts.

the catalytic behavior. The use of different preparation media can bring about two effects. On one hand, due to differences in the reactivity and reducibility of alcohol(s), the reaction mechanism between alcohol(s) and V_2O_5 can differ significantly, producing notable changes in the morphology of VPO precursor, the dispersion of VPO component, and the catalytic behavior of activated VPO [1–4,41]. With mixed iso-butyl/benzyl alcohols adopted as the reagent-solvent, V_2O_5 first reacted with

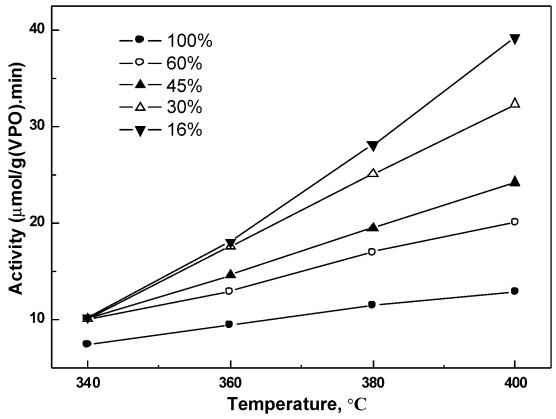

Fig. 10. Specific activities of VPO(m) and VPO/SBA-15(m) catalysts as a function of reaction temperature.

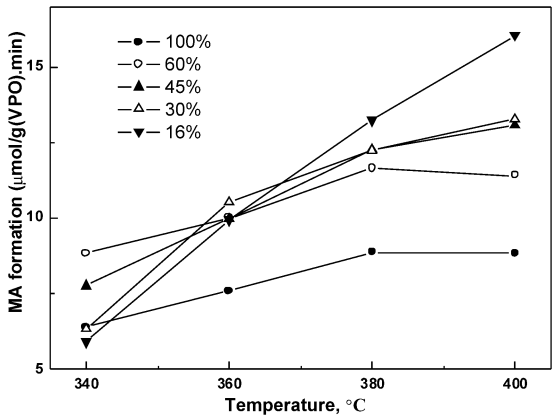

Fig. 11. MA formation rate over VPO(m) and VPO/SBA-15(m) catalysts on the basis of per unit mass of VPO species.

the aliphatic alcohol to form soluble vanadium (V) alkoxide, and then the vanadium (V) alkoxide species were reduced by benzyl alcohol to generate insoluble V_2O_4. With H_3PO_4 addition, the reduction was accelerated and completed with the creation of vanadyl acid phosphate [41]. When a single alcohol of iso-butanol was used, V_2O_5 reduction could hardly be accomplished before H_3PO_4 addition [41]. On the other hand, in different preparation media, there would be a difference in the aggregation of precursors and hence differences in the surface morphology of precursors. When generated in iso-butanol, the precursor usually showed a rosette-like morphology, whereas when generated in a benzyl alcohol-containing medium, morphology of platelets with stacking faults responsible for fine particle size, high dispersion on support, and better catalytic performance was observed [3,5].

The structure order or disorder of the final catalyst is determined largely by the nature of the precursor. Because the $VOHPO_4{\cdot}0.5H_2O$ precursor is a layered compound [3,6], intercalation of alcohol(s) into the precursor can occur, resulting in structure disorder in the direction perpendicular to the (001) plane [1,2,5,41]. The retention of benzyl alcohol in the "dried" precursor has been reported [7,41], with the structure disorder of the (001) plane increasing with increasing benzyl alcohol content in the mixed alcohols [7]. For the case of

supported VPO precursor derived in a single-alcohol medium, the well-ordered (001) plane of $VOHPO_4{\cdot}0.5H_2O$ is likely to be responsible for the formation of vanadium orthophosphates (γ-$VOPO_4$, α_1-$VOPO_4$, and $VOPO_4{\cdot}2H_2O$). It is speculated that the slow elimination of the intercalated aromatic molecules from VPO precursor can suppress the formation of excess V^{5+}-containing species.

4.2. The effect of support

SBA-15 has some unique properties, including very high surface area, large pore size, and high pore volume, that enable good dispersion of VPO component. MCM-41 and SBA-15 are both silica-based mesoporous materials with different pore sizes; the average pore diameter of the former is ca. 3 nm, whereas that of the latter is ca. 8 nm [31]. A comparison between VPO catalysts supported on MCM-41 and SBA-15 would provide insight into the VPO dispersion on the two supports. With Al-containing MCM-41 as the support, the (100) XRD peak was essentially maintained even at a VPO loading as high as 35% [33]. With SBA-15 as the support, the (100) diffraction peak diminished noticeably at 16% VPO loading (Fig. 3). Because the pores of SBA-15 are considerably larger than those of MCM-41, SBA-15 can accommodate more VPO components inside its pores, and hence the extent of loss in long-range order of hexagonal porosity is more notable. In the process of precursor loading, the soluble vanadium (V) alkoxide can be absorbed in the pores of SBA-15, and the insoluble V_2O_4 intermediate would then be produced and deposited inside the pores. With the addition of H_3PO_4, the subsequently generated $VOHPO_4{\cdot}0.5H_2O$ can be present inside the pores of SBA-15. At high VPO loadings, more VPO precursor of large particle size was generated outside the pores, that is, on the external surface of the support. The structure of loaded VPO was governed largely by the nature of the support material. When VPO components were loaded on supports of conventional SiO_2 [20], titania [21], and mesoporous Al-containing MCM-41 [33], they usually existed in amorphous form; however, the VPO supported on SBA-15 was found to be in crystalline form even at 16% loading. The large pores of SBA-15 (those $>$8.0 nm) favored the formation of large VPO entities. It should be pointed out that most of the mesopores in SBA-15 are ca. 8.3 nm (Fig. 2), notably larger than the value ($\sim$5 nm) calculated by BJH method (Table 1). These larger pores are spacious enough to accommodate VPO crystallites detected by XRD. Similar observations were made over VPO catalysts supported on both large-pore silica [32] and fumed SiO_2 [28] that have large primary pores ($\sim$10 nm) and secondary porosity, respectively; both were favorable for the formation of crystallized VPO. Moreover, the VPO entities located inside the SBA-15 mesopores should also contribute to the XRD signals of the $(VO)_2P_2O_7$ phase. Therefore, we propose that the supported VPO on SBA-15 can exist in crystallized form. On the other hand, some unique preparation procedures adopted in the present study, such as the addition of PEG additive in the preparation medium and controllable addition of H_3PO_4, are also responsible for enhancing the crystallinity of supported VPO [9] and suppressing the formation of excess V^{5+}-containing species [12,31]. Hutchings et al. [15] reported that unsupported amorphous VPO catalyst prepared through SCFD in CO_2 was nearly as active as its crystalline counterpart. However, supported VPO in the form of crystalline $(VO)_2P_2O_7$ generally performed better than that in the amorphous state [52].

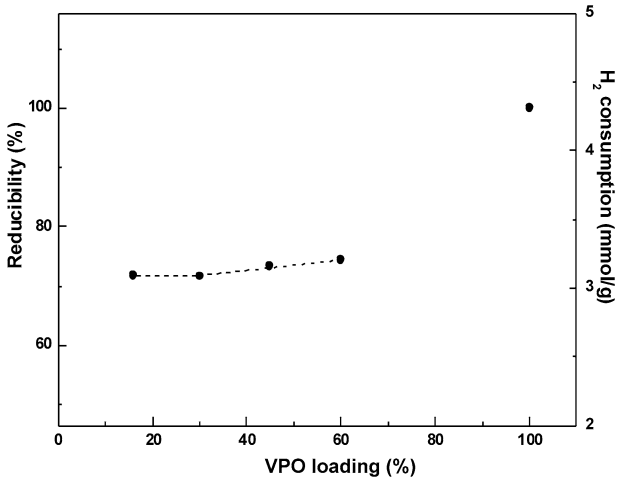

Fig. 12. Reducibility and H_2 consumption of VPO(m) and VPO/SBA-15(m) catalysts normalized to per unit mass of loaded VPO.

4.3. VPO–support interaction

Based on the extent of H_2 consumption in the TPR experiments (calibrated by CuO reduction), the reducibility of the supported VPOs was estimated. Note that the reducibility of serial VPO/SBA-15 catalysts was normalized on the basis of per unit mass of supported VPO (Fig. 12). Taking the reducibility of unsupported VPO as 100%, the reducibility was 71–74% for the supported VPO component at VPO loading of 16–60%. Because the supported VPOs are essentially crystalline $(VO)_2P_2O_7$, the change in reducibility of VPO component may be a result of VPO–support interaction. Due to the interaction of VPO species with silica, a portion of oxygen atoms at the interface are shared among the neighboring Si and V atoms, resulting in enhanced stability of the V atoms and decreased reducibility of VPO entities [20,33]. As illustrated by the TPR profiles (Fig. 7), the onset reduction temperature shifted to lower temperatures with increasing VPO loading, indicating a reduction in the extent of VPO–support interaction at higher VPO loadings.

The VPO–support interaction can have a notable impact on reaction performance. With a reducible support such as titania, the reducibility of supported VPO was enhanced due to strong VPO–titania interaction, and consequently there was an increase in activity but a decrease in selectivity [21]. When nonreducible silica was used as support, the VPO–silica interaction was relatively weak, and there was enhanced MA selectivity but reduced *n*-butane conversion [20]. It was also observed that the VPO–support interaction changed with surface property of silica, consequently affecting catalyst performance [25].

4.4. The phase composition

It is generally accepted that the structure of active phase (or sites) and the role of V^{5+} species are the key issues for the VPO-type catalysts [12–18]. Previously, crystalline $(VO)_2P_2O_7$ was proposed as the active phase for MA production [53,54], whereas that of $VOPO_4$ was thought to be active for CO_x formation [8]. However, it was generally observed that a VPO catalyst composed of $(VO)_2P_2O_7$ and a certain amount of $VOPO_4$ could be more active and selective for butane oxidation [55]. Centi et al. suggested that the V^{5+} species were involved in the redox cycle for *n*-butane oxidation, but excess (>5%) V^{5+} species would lead to deep oxidation of MA to carbon oxides [13]. The results of the present study also suggest that the performance of supported VPO catalysts is closely related to the phase composition of the VPO component. For example, when $VOPO_4$ phase (γ-$VOPO_4$, α_1-$VOPO_4$, or $VOPO_4{\cdot}2H_2O$) was present in a large quantity in the VPO/SBA-15(s) catalyst, both activity and selectivity declined appreciably.

The presence of $VOPO_4$ in either crystalline or amorphous form can notably affect the structure of the VPO component and, consequently, the reaction performance. The existence of $VOPO_4$ phase can change the stacking order of VPO, leading to VPO of smaller surface area and less active sites. A previous report indicated that through a water treatment, the surface area of a VPO catalyst could be enlarged from 9 to 31.5 m^2/g by the removal of soluble vanadium orthophosphate species [8]. The H_2-TPR results of VPO(s) and 45%VPO/SBA-15(s) suggest that the lattice oxygen related to V^{5+} species are reactive but not as selective, accounting for the low MA selectivities observed in Fig. 8. We propose that some supported VPO precursor can be easily transformed into $VOPO_4$ phases under in situ activation conditions. The V^{5+}-containing phases, including α_1-$VOPO_4$ and/or γ-$VOPO_4$, are generally present in supported VPO catalysts, especially in those prepared in aqueous media [19,23,25]. In the present study, a mixed iso-butyl/benzyl alcohol medium was found to be more suitable for the formation of crystalline $(VO)_2P_2O_7$ on the SBA-15 support; this is a key factor in achieving good MA yield.

5. Conclusion

In this study, for the first time a series of VPO catalysts supported on SBA-15 was prepared for *n*-butane oxidation to MA. When using mixed iso-butyl/benzyl alcohols as the reagent-solvent, the supported VPO species dispersed well on SBA-15 and existed mainly as crystalline $(VO)_2P_2O_7$. However, when using single iso-butanol as the reagent-solvent, the loaded VPO species were largely $VOPO_4$ phase (γ-$VOPO_4$, α_1-$VOPO_4$, and $VOPO_4{\cdot}2H_2O$), displaying significantly lower activity and MA selectivity. Different reaction mechanisms are responsible for the formation of VPO precursor in the different preparation media. The aggregation of precursor particles and the intercalation of alcohol molecules into the VPO precursors are critical factors affecting the phase composition and structural arrangement of the supported VPO component and, consequently, determining the performance of VPOs on SBA-15.

With the loading of VPO, the mesopores of SBA-15 were largely retained, but the long-range hexagonally ordered pore structure was considerably reduced, due to the intercalation of VPO species. TEM findings clearly indicated that a portion of the supported VPO components were located inside the pores of SBA-15. At high VPO loading (⩾30%), the VPO components were located predominantly on the external surface of SBA-15. In other words, the loaded VPO entities can exist as nanorods inside the channels and as large crystallites on the external surface of SBA-15. They are crystalline in nature and are detectable by XRD even at low VPO loadings. The XPS results confirmed that the oxidation state of surface vanadium was essentially +4 and that phosphate enrichment occurred on the sample surface. The Si:V ratios of different supported VPOs also demonstrated that VPO dispersion was a function of VPO loading. The results of H_2-TPR measurement suggested a VPO–support interaction that could lead to decreased reducibility of supported VPO.

In summary, fairly good catalytic activity was obtained when SBA-15 was used as a support for the VPO catalysts. At a typical reaction temperature of 673 K, the MA yields were 51, 44, and 30% over the 60, 45, and 30% VPO/SBA-15 catalysts, respectively. The unique properties of mesoporous SBA-15, the dispersion state and phase composition of VPO component, and the inherent interaction between VPO and support determine the overall catalyst performance.

Acknowledgments

This work was supported by RGC, Hong Kong Special Administration Region (grant HKBU 200103), and the research conducted at NJU was financed by the Chinese Ministry of Science and Technology (grant 2000048009).

References

[1] Y. Kamiya, S. Ueki, N. Hiyoshi, N. Yamamoto, T. Okuhara, Catal. Today 78 (2003) 281.
[2] M. O'Connor, B.K. Hodnett, Appl. Catal. 42 (1988) 91.
[3] J.B. Benziger, V. Guliants, S. Sundaresan, Catal. Today 33 (1997) 49.
[4] I.J. Ellison, G.J. Hutchings, M.T. Sananes, J.C. Volta, Chem. Commun. (1994) 1093.
[5] H.S. Horowitz, C.M. Blackstone, A.W. Sleight, G. Teufer, Appl. Catal. 38 (1988) 193.
[6] N. Hiyoshi, N. Yamamoto, T. Okuhara, Chem. Lett. (2001) 484.
[7] G. Busca, F. Cavani, G. Centi, F. Trifiro, J. Catal. 99 (1986) 400.
[8] V.V. Guliants, J.B. Benziger, S. Sundaresan, I.E. Wachs, J.M. Jehng, J.E. Roberts, Appl. Catal. A 28 (1996) 275.
[9] X.S. Wang, L.J. Xu, X. Chen, W.J. Ji, Q.J. Yan, Y. Chen, J. Mol. Catal. A 206 (2003) 261.
[10] M.J. Lorences, G.S. Patience, F.V. Díez, J. Coca, Appl. Catal. A 263 (2004) 193.
[11] F. Garbassi, J.C.J. Bart, R. Tassinari, G. Vlaic, P. Lagarde, J. Catal. 98 (1986) 317.
[12] C.J. Kiely, A. Burrows, G.J. Hutchings, K.E. Bere, J.C. Volta, A. Tuel, M. Abon, Faraday Discuss. 105 (1996) 103.
[13] G. Centi, F. Trifirò, J.R. Ebner, V.M. Franchetti, Chem. Rev. 88 (1988) 55.
[14] V.V. Guliants, J.B. Benziger, N.Y. Sundaresan, I.E. Wachs, Catal. Lett. 32 (1995) 379.
[15] G.J. Hutchings, J.A. Lopez-Sanchez, J.K. Bartley, J.M. Webster, A. Burrows, C.J. Kiely, A.F. Carley, C. Rhodes, M. Havecker, A. Knop-Gericke, R.W. Mayer, R. Schlogl, J.C. Volta, M. Poliakoff, J. Catal. 208 (2002) 197.

[16] R. Ebner, M.R. Thompson, Catal. Today 16 (1993) 51.
[17] H. Bluhm, M. Havecker, E. Kleimenov, A. Knop-Gericke, A. Liskowski, R. Schlogl, D.S. Su, Top. Catal. 23 (2003) 99.
[18] G.W. Coulston, S.R. Bare, H. Kung, K. Birkeland, G.K. Bethke, R. Harlow, N. Herron, P.L. Lee, Science 275 (1997) 191.
[19] K.E. Birkeland, S.M. Babitz, O.K. Bethke, H.H. Kung, G.W. Coulston, S.R. Bare, J. Phys. Chem. B 101 (1997) 6895.
[20] R.A. Overbeek, A.R.C.J. Pekelharing, A.J. van Dillen, J.W. Geus, Appl. Catal. A 135 (1996) 231.
[21] R.A. Overbeek, P.A. Warringa, M.J.D. Combag, L.M. Visser, A.J. van Dillen, J.W. Geus, Appl. Catal. A 135 (1996) 209.
[22] V.A. Zazhigalov, Y.P. Zaitsev, V.M. Belousov, B. Partitz, W. Hanke, G. Ohlmann, React. Kinet. Catal. Lett. 32 (1986) 209.
[23] W.D. Harding, K.E. Birkeland, H.H. Kung, Catal. Lett. 28 (1994) 1.
[24] J. Marc, C.C. Ledoux, P.H. Cuong, T. Vincent, K. Kostantinos, M. Patrick, L. Jan, J. Catal. 203 (2001) 495.
[25] J.M.C. Buenoa, G.K. Bethkeb, M.C. Kung, H.H. Kung, Catal. Today 43 (1998) 101.
[26] N.T. Do, M. Baerns, Appl. Catal. 45 (1988) 1.
[27] N.T. Do, M. Baerns, Appl. Catal. 45 (1988) 9.
[28] Z.Q. Zhou, H.Y. Xu, W.J. Ji, Y. Chen, Catal. Lett. 96 (2004) 221.
[29] C.T. Kresge, M.E. Leonowicz, W.J. Roth, J.C. Vartuli, J.S. Beck, Nature 359 (1992) 710.
[30] J.S. Beck, L.C. Vartuli, W.J. Roth, M.E. Leonowicz, C.T. Kresge, K.D. Schmitt, C.T.W. Chu, D.H. Olson, E.W. Sheppard, S.B. McMullen, J.B. Higgings, J.C. Schlenker, J. Am. Chem. Soc. 114 (1992) 10834.
[31] D. Zhao, J. Feng, Q. Huo, N. Melosh, G.H. Fredrickson, B.F. Chmelka, G.D. Stucky, Science 279 (1998) 548.
[32] W.Y. Nie, Z.Y. Wang, W.J. Ji, Y. Chen, C.T. Au, Appl. Catal. A 244 (2003) 265.
[33] W.Y. Nie, X.S. Wang, W.J. Ji, Q.J. Yan, Y. Chen, C.T. Au, Catal. Lett. 76 (2001) 3.
[34] E.A. Lombardo, C.A. Sanchez, L.M. Cornaglia, Catal. Today 15 (1992) 407.
[35] D. Ye, A. Satsuma, T. Hattor, Y. Mumkami, Catal. Today (1993) 113.
[36] F.B. Abdelouahab, R. Olier, N. Guilhaume, F. Lefebvre, J.C. Volta, J. Catal. 134 (1992) 151.
[37] F.J. Cabello Sanchez, J.A. Lopez-Sanchez, R.P.K. Wells, C. Rhodes, Catal. Lett. 77 (2001) 189.
[38] G. Landi, L. Lisi, J.C. Volta, Catal. Today 91–92 (2004) 275.
[39] Y. Kamiya, S. Ueki, N. Hiyoshi, N. Yamamoto, T. Okuhara, Catal. Today 78 (2003) 281.
[40] N. Harrouch Batis, H. Batis, A. Ghorbel, J.C. Vendrine, J.C. Volta, J. Catal. 128 (1991) 248.
[41] L.M. Cornaglia, C.A. Sanchez, E.A. Lombard, Appl. Catal. A 95 (1993) 117.
[42] W.J. Ji, L.J. Xu, X.S. Wang, Z. Hu, Q.J. Yan, Y. Chen, Catal. Today 74 (2002) 101.
[43] C.Y. Xiao, X. Chen, Z.Y. Wang, W.J. Ji, Y. Chen, C.T. Au, Catal. Today 93–95 (2004) 223.
[44] S. Jun, S.H. Joo, R. Ryoo, M. Kruk, M. Jaroniec, Z. Liu, T. Ohsuna, O. Terasaki, J. Am. Chem. Soc. 122 (2000) 10712.
[45] R. Ryoo, C.H. Ko, M. Kruk, V. Antochshuk, M. Jaroniec, J. Phys. Chem. B 104 (2000) 11465.
[46] Y.M. Liu, Y. Cao, N. Yi, W.L. Feng, W.L. Dai, S.R. Yan, H.Y. He, K.N. Fan, J. Catal. 224 (2004) 417.
[47] Y.M. Liu, Y. Cao, S.R. Yan, W.L. Dai, K.N. Fan, Catal. Lett. 88 (2003) 61.
[48] S.K. Hodnett, Catal. Rev. 27 (1985) 373.
[49] V.I. Bukhtiyarov, Catal. Today 56 (2000) 403.
[50] R.W. Wenig, G.L. Schrader, J. Phys. Chem. 90 (1986) 6480.
[51] M. Abon, J.C. Volta, Appl. Catal. A 157 (1997) 173.
[52] V.V. Guliants, Catal. Today 51 (1999) 255.
[53] B. Sciøtt, K.A. Jørgensen, R.J. Hoffmann, Phys. Chem. 95 (1991) 2297.
[54] J. Ziolkowski, E. Bordes, P.J. Courtine, J. Mol. Catal. 84 (1993) 307.
[55] J.C. Volta, Catal. Today 32 (1996) 29.